Theoretical calculation of a full-dimensional *ab initio* potential energy surface and prediction of infrared spectra for Xe–CS$_2$

Miao Qin,†[ab] Xiuchan Xiao 🔟†*[ab] and Hua Zhu[c]

An effective four-dimensional (4D) *ab initio* potential energy surface (PES) for Xe–CS$_2$ which explicitly involves the intramolecular Q_1 symmetric stretching and Q_3 antisymmetric stretching vibrational coordinates of CS$_2$ is constructed. The computations are carried out employing single- and double-excitation coupled-cluster theory with a non-iterative perturbation treatment of triple excitations [CCSD(T)] method with a large basis set. Two vibrationally averaged potentials at the ground and $\nu_1 + \nu_3$ ($\nu_1 = 1$, $\nu_3 = 1$) excited states are obtained by integrating the 4D potentials over the Q_1 and Q_3 coordinates. The potentials have a T-shaped global minimum and two equivalent linear local minima. The radial discrete variable representation/angular finite basis representation and the Lanczos algorithm are employed to calculate the rovibrational energy levels for Xe–CS$_2$. The infrared band origin shift associated with the fundamental band of CS$_2$ is predicted, which is red-shifted by -1.996 cm^{-1} in the $\nu_1 + \nu_3$ region. In addition, we further predict the spectroscopic parameters for the ground and the $\nu_1 + \nu_3$ excited states of Xe–CS$_2$. Compared with the previous Rg–CS$_2$ (Rg = He, Ne, Ar, Kr) complexes, we found that the complexes of the rare gas atoms with CS$_2$ display obvious regularities.

I. Introduction

The linear CX$_2$ (X = O, S) molecules play an important role in the investigation of atmosphere. While complexes consisting of small linear molecules (CO$_2$, OCS, CS$_2$) bound to a rare gas (Rg) have had a remarkable growth in interest in spectroscopic studies. Such studies are aimed at advancing our understanding of the weak intermolecular forces and dynamics of these bound molecules. As we know, CO$_2$ exists extensively in nature and absorbs infrared radiation in the ground. Accordingly, complexes containing CO$_2$ have been widely investigate both experimentally[1–7] and theoretically.[8–25] As an analog of CO$_2$, CS$_2$ is one of the sulfur compounds in the Earth's atmosphere and has also been widely studied because sulfur is a key element in the spectroscopy of giant planets. In addition, some interesting differences were explored for Rg–CS$_2$ compared to Rg–CO$_2$.

Experimentally, the first infrared spectra for the Rg–CS$_2$ complexes[26] with Rg = He, Ne, Ar were studied in the CS$_2$ ν_3 region. Meanwhile, Mivehvar *et al.* also reported the high resolution spectra of the He–CS$_2$ complex in the $\nu_1 + \nu_3$ region (2185 cm^{-1}). In their work, the structures were T-shaped and the

spectroscopic parameters were presented. Theoretically, a number of *ab initio* potential energy surfaces (PESs) for Rg–CS$_2$ were constructed at different levels of theory. For instance, Farrokhpour and co-workers[27] first determined the PESs for the Rg–CS$_2$ complexes using CCSD(T) theory with the aug-cc-pVDZ basis set. Soon after, Zang *et al.*[28] reported the two-dimensional PES for the Rg–CS$_2$ (Rg = He, Ne, Ar) complexes by using the aug-cc-pVTZ basis set at the CCSD(T) level. However, these theoretical studies have obtained the PESs that encompass only two intermolecular vibration coordinates and a fixed CS$_2$ geometry. The results showed that the spectral pattern in the infrared region cannot be properly identified. Thus, construction of the PESs that involve the intramolecular vibration modes of CS$_2$ is needed. Recently, we calculated a 3D PES of the Rg–CS$_2$ complex[29,30] including the antisymmetric stretching Q_3 coordinate of the CS$_2$ monomer, and showed a good agreement with the experimental infrared data. In order to explore more detailed spectral information for Rg–CS$_2$, we further carried out the calculation of a four-dimensional PES of the Rg–CS$_2$ (ref. 31–33) complexes, which incorporates the Q_1 symmetric and Q_3 anti-symmetric stretching coordinates of CS$_2$. We have successfully reported the 4D PESs for the complexes of the lighter rare gas atoms with CS$_2$ by this method. To our knowledge, the experimental and theoretical information in the $\nu_1 + \nu_3$ region are absent for Xe–CS$_2$.

In order to discover the trends and diversities among the Rg–CS$_2$ complexes, we present a reliable 4D PES for Xe–CS$_2$ with CS$_2$ in the $\nu_1 + \nu_3$ region by applying the CCSD(T) method with the

[a]School of Architectural and Environmental Engineering, Chengdu Technological University, Chengdu 611730, China. E-mail: shawailsa@sina.cn

[b]Center of Big Data for Smart Environmental Protection, Chengdu Technological University, Chengdu 611730, China

[c]School of Chemistry, Sichuan University, Chengdu 610064, China

† Miao Qin and Xiuchan Xiao contributed equally to this work.

aug-cc-pVQZ basis set. This paper is arranged as follows: in Section II, we show the computational details that include *ab initio* and rovibrational energy levels. The discussion of the PES, the calculated rovibrational bound states, and the predicted infrared spectra are presented in Sections III–IV. Finally, a brief conclusion is given in Section V.

II.   Computational details

A.   *Ab initio* calculations

For the Xe–CS$_2$ dimer, the Jacobi coordinates (R, θ, Q_1, Q_3) are employed to describe the geometry. In the geometric variables, R denotes the intermolecular distance between the center of mass of CS$_2$ to the Xe atom, the angle of the vector R with respect to the CS$_2$ molecule is defined as θ. Q_1 and Q_3 are the normal mode coordinates, which describe the ν_1 symmetric stretching vibration and ν_3 antisymmetric stretching vibration of CS$_2$, respectively. Here, the intramolecular vibrational coordinates (Q_1, Q_3) can be simply defined as

$$Q_1 = \left(r_{CS_1} + r_{CS_2} - 2r_e\right)\big/\sqrt{2} \tag{1}$$

$$Q_3 = \left(r_{CS_1} - r_{CS_2}\right)\big/\sqrt{2} \tag{2}$$

where r_{CS_1} and r_{CS_2} mean the two C–S bond lengths of CS$_2$, r_e is the average bond length derived from experimental spectra data.[34] The two-dimensional Q_1 and Q_3 potential curves were computed at the CCSD(T) level to determine the energy levels and wave functions for the Q_1 and Q_3 modes. The coordinate scaling method[35] was employed to adjust the two-dimensional potential in order to reproduce the experimental frequencies for the fundamental band.[34] We generated 25 potential optimized discrete variable representation (PODVR)[36,37] grid points corresponding to $Q_1 = -0.122411, -0.044046, -0.027968, -0.101203, -183772a_0$, $Q_3 = -0.245743, -0.116813, 0.0, 0.116813, 0.245743a_0$ for the ground state, and $Q_1 = -0.139155, -0.060791, 0.011220, 0.084454, 0.167022a_0$, $Q_3 = -0.247934, -0.117859, 0.0, 0.117859, 0.247934a_0$ for the $\nu_1 + \nu_3$ $(\nu_1 = 1, \nu_3 = 1)$ excited state.

The *ab initio* potential energies were computed for a total of about 9000 discrete points. A relatively dense grid was calculated with 27 values of R ranging from $5.50a_0$ to $24.00a_0$ and 13 points of θ from $0°$ to $180°$ at intervals of $15°$. The four dimensional PES for Xe–CS$_2$ was performed using the CCSD(T)[38] method. The aug-cc-pVQZ basis set of Woon and Dunning[39] was used for carbon and sulfur atoms, and the quasirelativistic pseudopotential aug-cc-pVQZ-PP[40] basis set was used for the Xe atom, supplemented with an additional set of bond functions (3s3p2d1f1g).[41] The full counterpoise procedure (FCP)[42] was selected to correct the basis set superposition error (BSSE). The vibrationally averaged 2D potentials $V_{\nu_1+\nu_3}(R,\theta)$ were obtained by averaging the 4D potential over the Q_1 and Q_3 vibrational coordinates, which can be written as

$$V_{\nu_1+\nu_3}(R, \theta) =$$

$$\int_{-\infty}^{\infty} \psi_{\nu_1+\nu_3}(Q_1, Q_3) V(R, \theta, Q_1, Q_3) \psi_{\nu_1+\nu_3}(Q_1, Q_3) \mathrm{d}Q_1 \mathrm{d}Q_3 \tag{3}$$

The cubic spline interpolation was employed to generate the averaged PESs for R and θ coordinates. The root-mean-square (rms) deviation is about 0.08 cm^{-1} in the final fit. All calculations were carried out using the MOLPRO package.[43]

B.   Calculations of rovibrational energy levels

With the Born–Oppenheimer approximation, the vibrational averaged 2D intermolecular Hamiltonian of the Xe–CS$_2$ complex can be written as[44,45]

$$\hat{H} = -\frac{1}{2\mu}\frac{\partial^2}{\partial R^2} + \frac{\hat{j}^2}{2I_{\nu_1+\nu_3}} + \frac{\left(\hat{J} - \hat{j}\right)^2}{2\mu R^2} + V_{\nu_1+\nu_3}(R, \theta) \tag{4}$$

where μ is the reduced mass of the Xe–CS$_2$ complex, $\hat{J}$ and $\hat{j}$ are the angular momentum operators for the total and monomer rotations. $I_{\nu_1+\nu_3}$ represents the vibrationally averaged rotational moment of the inertia of CS$_2$, which can be defined by the following equation,

$$I_{\nu_1+\nu_3} = \int_{-\infty}^{\infty} \psi_{\nu_1+\nu_3}(Q_1, Q_3) I_{Q_1+Q_3} \psi_{\nu_1+\nu_3}(Q_1, Q_3) \mathrm{d}Q_1 \mathrm{d}Q_3 \tag{5}$$

Based on the PES, the rovibrational Hamiltonian and wave functions were calculated with the radial DVR/angular FBR method.[46,47] In our work, 120 sine-DVR[48] grid points were used for the radial coordinate R. For the angular coordinate, we selected 90 DVR grids and 89 basis functions of associated Legendre polynomials. The Lanczos algorithm method[49,50] was used to diagonalize the Hamiltonian matrix, and we selected 10 000 Lanczos iterations to obtain the eigenvalues and eigenvectors. For the angular part, the parity-adapted rotational basis for the three Euler angles (α,β,γ) can be written as

$$C_{KM}^{Jp}(\alpha, \beta, \gamma) = [2(1 + \delta_{K0})]^{-1/2} \big[D_{MK}^{J*}(\alpha, \beta, \gamma) + (-1)^{J+K+p} D_{M-K}^{J*}(\alpha, \beta, \gamma)\big], \quad p = 0, 1 \tag{6}$$

where $D_{MK}^{J}(\alpha, \beta, \gamma)$ were the normalized rotational functions for Xe–CS$_2$, the space-inversion parity $p = 0$ or 1 illustrates that the basis is even or odd under inversion. The total parity was given by $(-1)^{J+P}$.

III.   Potential energy surface

The contour plot of the vibrationally averaged 2D $\nu_1 + \nu_3$ excited state PES is showed in Fig. 1, which clearly displays that the global minimum is a T-shaped configuration at $R = 3.97$ Å and $\theta = 90.0°$ with a well depth of 413.875 cm^{-1}. In addition, there are two equivalent linear local minima at $R = 5.56$ Å and $\theta = 0°$ or $180°$ with a depth of 248.045 cm^{-1}. In our PES, between the two minima, there are two saddle points with an energy barrier of 187.997 cm^{-1} relative to the global minimum, located at $R = 5.08$ Å and $\theta = 45°$ or $135°$. In order to compare the Xe–CS$_2$ complex with the other Rg–CS$_2$ complexes, the differences in the geometries and well depths between the Rg–CS$_2$ complexes[31–33,51,52] are listed in Table 1. One can see that the Rg–CS$_2$ complexes have similar shapes, such as the T-shaped global minimum, two linear local minima, and two saddle points.
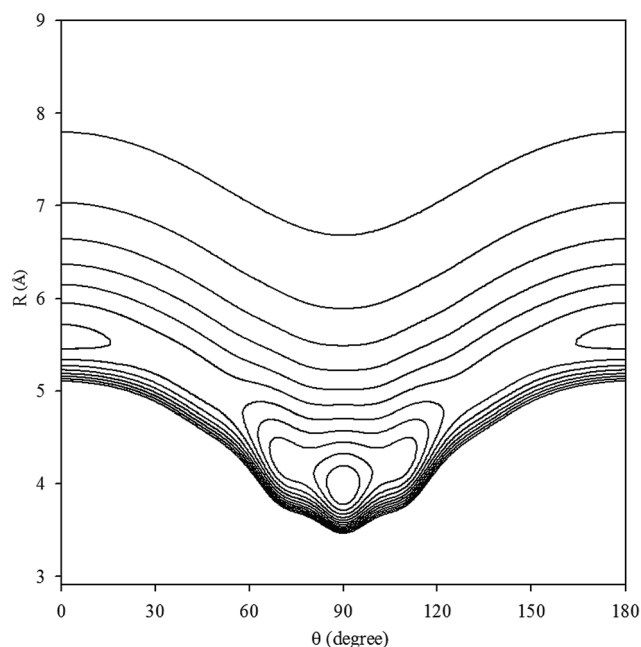
Fig. 1 Contour plot (in cm^{-1}) of the averaged intermolecular potential energy surface for Xe−CS$_2$ with CS$_2$ at the $\nu_1 + \nu_3$ excited state.

Table 2 The calculated energy levels (in cm^{-1}) for the first twenty vibrational bound states of Xe−CS$_2$ with CS$_2$ at the ground and the $\nu_1 + \nu_3$ excited states

Ground state				ν_5 state			
N		N		N		N	
0	−372.243	10	−276.947	0	−374.239	10	−278.046
1	−340.903	11	−275.624	1	−342.887	11	−276.971
2	−330.927	12	−273.955	2	−335.591	12	−275.602
3	−312.666	13	−266.022	3	−314.627	13	−266.029
4	−308.886	14	−258.545	4	−310.894	14	−259.381
5	−308.813	15	−257.516	5	−310.755	15	−259.247
6	−298.008	16	−256.517	6	−299.059	16	−256.907
7	−295.275	17	−252.014	7	−296.373	17	−253.608
8	−284.470	18	−251.523	8	−285.564	18	−253.276
9	−283.164	19	−245.973	9	−284.769	19	−246.196

However, there are some deviations among the Rg−CS$_2$ complexes. For example, the depth of the global and local minima become deeper from He−CS$_2$ to Xe−CS$_2$, which indicates the intermolecular interactions become stronger with the increasing mass of the rare gas atom. For another, the well depth of Xe−CS$_2$ is much larger than the other Rg−CS$_2$ complexes, which means the Xe atom is strongly hindered from free motion around the CS$_2$ molecule. In addition, the minimum energy distance gradually become larger from He−CS$_2$ to Xe−CS$_2$. Compared with the previous theoretical study of the potential,[51] the contour plots look almost the same as those for our work, and the positions and energies of the stationary points are shifted only slightly.

IV. Bound states of rovibrational energy levels and infrared spectra

Based on the potential, the energy levels of the bound states were calculated. In order to simplify our writing, we label the $\nu_1 + \nu_3$ of CS$_2$ as the ν_5 vibrational state for Xe−CS$_2$. In Table 2, we display the first twenty pure vibrational bound states of the Xe−

CS$_2$ complex for the ground and ν_5 states of CS$_2$. As seen in Table 2, the first bound state for the ν_5 state is −374.239 cm^{-1}, which reveals the zero-point energy is 39.636 cm^{-1} relative to global minimum, only about one-tenth of the global well depths. Due to the deep well and high barrier for Xe−CS$_2$, the bound states are much deeper than the other Rg−CS$_2$ complexes.[31–33,52] The $\nu_1 + \nu_3$ band origin shift is determined by $\Delta\nu = E_0^5 - E_0^0$,[53] where E_0^ν are the ground state energies of Xe−CS$_2$ with the CS$_2$ monomer in the corresponding ν vibrational state. Meanwhile, we further predicted the infrared band origin shift of Xe−CS$_2$, which is −1.996 cm^{-1} indicating that is negative (red-shift) in sign and large in magnitude. In addition, the band origin shifts of the other Rg−CS$_2$ complexes[26,29–33,51,52] are listed in Table 3, together with the Rg−CO$_2$ complexes.[2,6] One can see that the tendency of the CS$_2$ shifts are similar to CO$_2$. Besides, the results indicate the lighter complexes (He, Ne) tend to positive (blue shifts), while the larger complexes (Ar, Kr, Xe) tend to negative (red-shifts). The predicted $\nu_1 + \nu_3$ band shift for Xe−CS$_2$ (−1.996 cm^{-1}) is larger than that for Xe−CO$_2$ (−1.447 cm^{-1}), revealing that Xe−CS$_2$ has a larger weakening of the vdW bond upon vibrational excitation in the $\nu_1 + \nu_3$ region.

In Fig. 2, we present the contour plots of the wave functions of Xe−CS$_2$ with CS$_2$ at the ground state. It is clear from Fig. 2 that the vibrational ground state is localized around the T-shaped global minimum. The first two vibrational excited states are characterized predominantly by bending and stretching vibrations, respectively, while the corresponding wave functions are distributed and exhibit a strong mixing between the bending and stretching vibration modes for the higher vibrational

Table 1 The stationary geometries (Å and deg) and well depths (cm^{-1}) of Rg−CS$_2$ (Rg = He, Ne, Ar, Kr, Xe)

Rg−CS$_2$	Global minimum	Local minimum	Saddle point
He−CS$_2$ (ref. 31)	(3.36, 90, −52.68)	(5.00, 0/180, −32.11)	(4.56, 59/121, −21.39)
Ne−CS$_2$ (ref. 33)	(3.44, 90, −104.35)	(5.03, 0/180, −67.15)	(4.56, 44/136, −51.12)
Ar−CS$_2$ (ref. 32)	(3.68, 90, −279.77)	(5.26, 0/180, −173.47)	(4.92, 39/141, −146.75)
Kr−CS$_2$ (ref. 52)	(3.76, 90, −367.06)	(5.39, 0/180, −226.16)	(4.92, 45/135, −203.49)
Xe−CS$_2$ (ref. 51)	(3.97, 90, −414.77)	(5.56, 0/180, −243.66)	(5.08, 46/134, −224.37)
Xe−CS$_2$	(3.97, 90, −413.88)	(5.56, 0/180, −248.04)	(5.08, 45/135, −225.88)

Table 3 The vibrational shifts of band origin for Rg–CS$_2$, compared with Rg–CO$_2$ (in cm^{-1})

	CO$_2$ ν_3	CS$_2$ ν_3	CS$_2$ $\nu_1 + \nu_3$
He	+0.095 (ref. 6)	+0.108 (ref. 26)	+0.228 (ref. 31)
Ne	+0.130 (ref. 2)	+0.180 (ref. 26)	+0.251 (ref. 33)
Ar	−0.470 (ref. 2)	+0.067 (ref. 26)	−0.049 (ref. 32)
Kr	−0.884 (ref. 2)	−0.787 (ref. 51)	−1.236 (ref. 52)
Xe	−1.447 (ref. 2)	−1.066 (ref. 51)	−1.996

excited states. The calculated average distance $\langle R \rangle$ and the average angle $\langle \theta \rangle$ for the ground state are 3.99 Å and 87.85°, respectively, which is very close to the global minimum ($R = 3.97$ Å and $\theta = 90°$). The radial dispersion $\sqrt{\langle R^2 \rangle - \langle R \rangle^2}$ and angular dispersion $\sqrt{\langle \theta^2 \rangle - \langle \theta \rangle^2}$ are 0.14 Å and 2.15°, respectively. Therefore, the ground state is rigid.

The rovibrational energies of Xe–CS$_2$ are labeled by the asymmetric rotor quantum numbers J_{KaKc}, where J denotes the total angular momentum, K_a and K_c represent the projections of J onto the a and c principal axes of inertia. The rovibrational energy levels consist of four blocks, (even/even), (even/odd),

(odd/even), and (odd/odd) for different combination parity of (j/p). The rovibrational energies of Xe–CS$_2$ for the vibrational ground and $\nu_1 + \nu_3$ excited states are shown in Table 4, and the total angular momentum J ranges from 0 to 5.

The rovibrational energy levels within $J \leq 3$ are used to fit to a Watson asymmetric top Hamiltonian[54] employing the a-type reduction in the I^r representation,

$$
\begin{aligned}
H = {} & \frac{1}{2}(B+C)J^2 + \left[A - \frac{1}{2}(B+C)\right]J_a^2 + \frac{1}{2}(B-C)\left(J_b^2 - J_c^2\right) \\
& - \Delta_J J^4 - \Delta_{JK} J_a^2 J^2 - \Delta_K J_a^4 - 2\delta_J J^2 \left(J_b^2 - J_c^2\right) \\
& - \delta_K\left[J_a^2\left(J_b^2 - J_c^2\right) + \left(J_b^2 - J_c^2\right)J_a^2\right]
\end{aligned}
$$

(7)

The fitted molecular spectroscopic constants for the Xe–CS$_2$ complex are given in Table 5. Because the energy levels for Xe–CS$_2$ at the ground state are almost equal to the $\nu_1 + \nu_3$ excited state, the molecular parameters of the two states are very similar. The calculated inertial defects Δ_0 of this complex with CS$_2$ at the ground state and the $\nu_1 + \nu_3$ excited state are around 1.07 amu Å^2 and 1.13 amu Å^2, respectively. For Rg–CS$_2$ (Rg = He,[31] Ne,[33] Ar,[32] Kr[52]), the inertial defects Δ_0 in the ground state
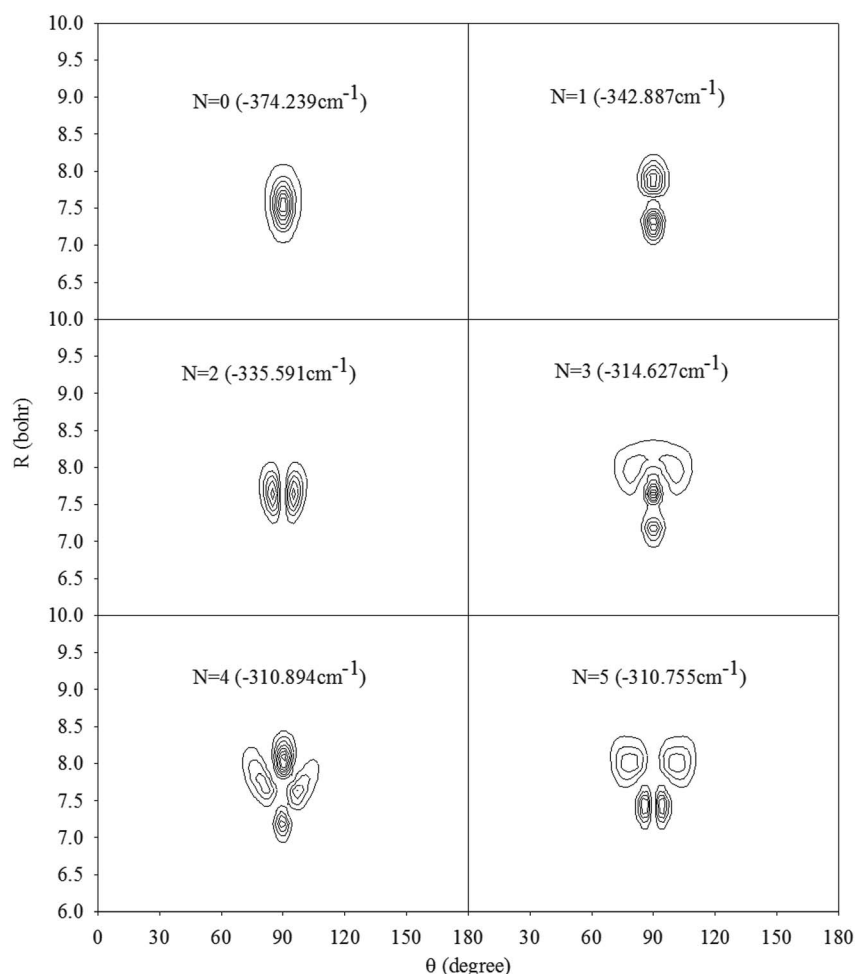

Fig. 2 Contour plots of the wave functions for the lowest six vibrational states of Xe–CS$_2$ with CS$_2$ at the $\nu_1 + \nu_3$ excited state.

Table 4 The rovibrational energy levels (in cm^{-1}) of Xe–CS$_2$ with CS$_2$ at the ground and $\nu_1 + \nu_3$ excited states

Level	J	E (J_{KaKc}) Even/Even	Even/Odd	Odd/Even	Odd/Odd
Ground state	0	−372.243 (0_{00})			
	1		−372.203 (1_{01})	−372.113 (1_{10})	−372.116 (1_{11})
	2	−372.122 (2_{02})	−371.770 (2_{21})	−372.040 (2_{12})	−372.028 (2_{11})
		−371.769 (2_{20})			
	3	−371.649 (3_{22})	−372.002 (3_{03})	−371.902 (3_{12})	−371.925 (3_{13})
		−371.648 (3_{21})		−371.207 (3_{30})	−371.208 (3_{31})
	4	−371.843 (4_{04})	−371.488 (4_{23})	−371.772 (4_{14})	−371.734 (4_{13})
		−371.487 (4_{22})	−370.430 (4_{41})	−371.047 (4_{32})	−371.046 (4_{31})
		−370.430 (4_{40})			
	5	−371.288 (5_{24})	−371.644 (5_{05})	−371.525 (5_{14})	−371.580 (5_{15})
		−370.229 (5_{42})	−371.284 (5_{23})	−370.846 (5_{32})	−370.846 (5_{33})
			−370.229 (5_{41})	−369.436 (5_{50})	−369.436 (5_{51})
ν_5 state	0	−374.239 (0_{00})			
	1		−374.199 (1_{01})	−374.110 (1_{10})	−374.114 (1_{11})
	2	−374.119 (2_{02})	−373.770 (2_{21})	−374.037 (2_{12})	−374.026 (2_{11})
		−373.770 (2_{20})			
	3	−373.650 (3_{22})	−373.999 (3_{03})	−373.900 (3_{12})	−373.923 (3_{13})
		−373.649 (3_{21})		−373.213 (3_{30})	−373.214 (3_{31})
	4	−373.839 (4_{04})	−373.489 (4_{23})	−373.770 (4_{14})	−373.732 (4_{13})
		−373.487 (4_{22})	−372.442 (4_{41})	−373.053 (4_{32})	−373.052 (4_{31})
		−372.442 (4_{40})			
	5	−373.288 (5_{24})	−373.641 (5_{05})	−373.522 (5_{14})	−373.579 (5_{15})
		−372.241 (5_{42})	−373.284 (5_{23})	−372.851 (5_{32})	−372.852 (5_{33})
			−372.241 (5_{41})	−371.456 (5_{50})	−371.456 (5_{51})

Table 5 The calculated spectroscopic constants (in cm^{-1}) and the inertial defects Δ_0 (in amu Å^2) for the Xe–CS$_2$ complex with CS$_2$ at the ground and the $\nu_1 + \nu_3$ excited states

	Ground state	ν_5 state
A	0.108321	0.107674
B	0.022038	0.022023
C	0.018291	0.018261
Δ_K	-2.443×10^{-7}	-3.110×10^{-7}
Δ_{JK}	3.748×10^{-7}	3.258×10^{-7}
Δ_J	4.563×10^{-6}	8.778×10^{-6}
δ_K	2.050×10^{-6}	2.225×10^{-6}
δ_J	9.176×10^{-9}	2.993×10^{-9}
Δ_0	1.07	1.13

were found to be 6.14, 3.09, 2.93, 2.32 amu Å^2, respectively. The decrease in the inertial defects reveals that the vdW complexes are more rigid with the increase in the mass of the rare gas atom. The asymmetry parameter κ, $\kappa = (2B - A - C)/(A - C)$ (equal to -1 for the symmetric prolate top) is -0.917 and -0.916 for this complex with CS$_2$ at the ground and the $\nu_1 + \nu_3$ excited states, respectively.

V. Conclusions

In this paper, a new four-dimensional potential energy surface for the Xe–CS$_2$ complex including the Q_1 and Q_3 normal modes was constructed. We calculated the intermolecular potential with five PODVR grid points for the Q_1 and Q_3 normal modes, respectively, using the CCSD(T) method with the aug-cc-pVQZ basis set plus bond functions. Based on the *ab initio* potential points, two vibrationally averaged PESs of the Xe–CS$_2$ complex were generated. We found that each potential energy surface has a T-shaped global minimum and two equivalent local linear minima. The bound rovibrational energy levels of Xe–CS$_2$ were obtained by employing the radial DVR/angular FBR method and the Lanczos algorithm. The predicted band origin shift is -1.996 cm^{-1}. Meanwhile, we found that the Rg–CS$_2$ complexes have very similar features. For example, each PES is characterized by a T-shaped global minimum. For another, the regularities were represented among the complexes from He–CS$_2$ to Xe–CS$_2$. It is expected that the work on the Rg–CS$_2$ complexes in the $\nu_1 + \nu_3$ region of CS$_2$ should be useful for further theoretical and experimental studies.

Conflicts of interest

There are no conflicts to declare.

Acknowledgements

References

1 G. T. Fraser, A. S. Pine and R. D. Suenram, *J. Chem. Phys.*, 1988, **88**, 6157.

2 R. W. Randall, M. A. Walsh and B. J. Howard, *Faraday Discuss. Chem. Soc.*, 1988, **85**, 13.

3 M. Iida, Y. Ohsbima and Y. Endo, *J. Phys. Chem.*, 1993, **97**, 357.

4 A. S. Pine and G. T. Fraser, *J. Chem. Phys.*, 1988, **89**, 100.

5 T. Konno, S. Fukuda and Y. Ozaki, *Chem. Phys. Lett.*, 2006, **421**, 421.

6 M. J. Weida, J. M. Sperhac and D. J. Nesbitt, *J. Chem. Phys.*, 1994, **101**, 8351.

7 Y. J. Xu and W. Jäger, *J. Mol. Spectrosc.*, 1998, **192**, 435.

8 G. A. Parker, M. Keil and A. Kuppermann, *J. Chem. Phys.*, 1983, **78**, 1145.

9 M. Keil and G. A. Parker, *J. Chem. Phys.*, 1985, **82**, 1947.

10 L. Beneventi, P. Casavecchia, F. Vecchiocattivi, G. G. Volpi, U. Buck, C. Lauenstein and R. Schinke, *J. Chem. Phys.*, 1988, **89**, 4671.

11 C. F. Roche, A. Ernesti, J. M. Huston and A. S. Dickinson, *J. Chem. Phys.*, 1996, **104**, 2156.

12 P. J. Marshall, M. M. Szczesniak, J. Sadlej, G. Chalasinski, M. A. ter Horst and C. J. Jameson, *J. Chem. Phys.*, 1996, **104**, 6569.

13 J. M. Hutson, A. Ernesti, M. M. Law, C. F. Roche and R. J. Wheatley, *J. Chem. Phys.*, 1996, **105**, 9130.

14 G. S. Yan, M. H. Yang and D. Q. Xie, *J. Chem. Phys.*, 1998, **109**, 10284.

15 F. Negri, F. Ancliotto, G. Mistura and F. Toigo, *J. Chem. Phys.*, 1999, **111**, 6439.

16 H. Ran and D. Q. Xie, *J. Chem. Phys.*, 2008, **128**, 124323.

17 Y. L. Cui, H. Ran and D. Q. Xie, *J. Chem. Phys.*, 2009, **130**, 224311.

18 R. Chen, E. Q. Jiao, H. Zhu and D. Q. Xie, *J. Chem. Phys.*, 2010, **133**, 104302.

19 R. Chen and H. Zhu, *J. Theor. Comput. Chem.*, 2012, **11**, 1175.

20 R. Chen, H. Zhu and D. Q. Xie, *Chem. Phys. Lett.*, 2011, **511**, 229.

21 M. Chen and H. Zhu, *J. Theor. Comput. Chem.*, 2012, **11**, 537.

22 H. Li and R. J. Le Roy, *Phys. Chem. Chem. Phys.*, 2008, **10**, 4128.

23 H. Li, N. Blinov, P.-N. Roy and R. J. Le Roy, *J. Chem. Phys.*, 2009, **130**, 144305.

24 Y. L. Cui, H. Ran and D. Q. Xie, *J. Theor. Comput. Chem.*, 2008, **7**, 707.

25 C. J. Xie, R. Chen, H. Zhu and D. Q. Xie, *Chem. Res. Chin. Univ.*, 2009, **9**, 1851.

26 F. Mivehvar, C. Lauzin, A. R. W. McKellar and N. Moazzen-Ahmadi, *J. Mol. Spectrosc.*, 2012, **281**, 24.

27 H. Farrokhpour and M. Tozihi, *Mol. Phys.*, 2013, **111**, 779.

28 L. M. Zang, W. Dai, L. M. Zheng, C. X. Duan, Y. P. Lu and M. H. Yang, *J. Chem. Phys.*, 2014, **140**, 114310.

29 T. Yuan and H. Zhu, *Theor. Chem. Acc.*, 2014, **133**, 1537.

30 T. Yuan, X. L. Sun, Y. Hu and H. Zhu, *J. Chem. Phys.*, 2014, **141**, 104306.

31 J. Shang, T. Yuan and H. Zhu, *Theor. Chem. Acc.*, 2016, **135**, 1.

32 J. Shang, T. Yuan and H. Zhu, *Chem. Phys. Lett.*, 2016, **648**, 147.

33 M. Qin, J. Shang, Q. Hong and H. Zhu, *Mol. Phys.*, 2017, **115**, 379.

34 J. S. Wells, M. Schneider and A. G. Maki, *J. Mol. Spectrosc.*, 1988, **132**, 422.

35 J. M. Bowman and B. Gazdy, *J. Chem. Phys.*, 1991, **94**, 816.

36 H. Wei and T. Carrington, *J. Chem. Phys.*, 1992, **97**, 3029.

37 J. Echave and D. C. Clary, *Chem. Phys. Lett.*, 1992, **190**, 225.

38 M. Meuwly and J. M. Hutson, *J. Chem. Phys.*, 2003, **119**, 8873.

39 D. E. Woon and T. H. Dunning, *J. Chem. Phys.*, 1993, **98**, 1358.

40 K. A. Peterson, D. Figgen, E. Goll, H. Stoll and M. Dolg, *J. Chem. Phys.*, 2003, **119**, 11113.

41 T. B. Pedersen, B. Fernandez, H. Koch and J. Makarewicz, *J. Chem. Phys.*, 2001, **115**, 8431.

42 S. F. Boys and F. Bernardi, *Mol. Phys.*, 1970, **19**, 553.

43 H. J. Werner, P. J. Knowles, R. D. Amos, A. Berning, D. L. Cooper, M. J. O. Deegan, A. J. Dobbyn, F. Eckert, S. T. Elbert, C. Hampel, R. Lindh, A. W. Lloyd, W. Meyer, A. Nicklass, K. Peterson, R. Pitzer, A. J. Stone, P. R. Taylor, M. E. Mura, P. Pulay, M. Schutz, H. Stoll and T. Thoorstcinsso, *Molpro, version 2000.1, a package of ab initio programs*, 2000, see http://www.molpro.net.

44 J. Tennyson and B. T. Sutcliffe, *Mol. Phys.*, 1984, **51**, 887.

45 S. Miller and J. Tennyson, *J. Mol. Spectrosc.*, 1988, **128**, 530.

46 S. Y. Lin and H. Guo, *J. Chem. Phys.*, 2002, **117**, 5183.

47 R. Q. Chen, G. B. Ma and H. Guo, *Chem. Phys. Lett.*, 2000, **320**, 567.

48 D. T. Colbert and W. H. Miller, *J. Chem. Phys.*, 1992, **96**, 1982.

49 C. J. Lanczos, *J. Res. Natl. Bur. Stand.*, 1950, **45**, 255.

50 H. G. Yu, *J. Chem. Phys.*, 2002, **117**, 8190.

51 T. Yuan, M. L. Yang and H. Zhu, *Comput. Theor. Chem.*, 2015, **88**, 1070.

52 Q. Hong, M. Qin and H. Zhu, *Acta Chim. Sin.*, 2018, **76**, 138.

53 F. Paesani and K. B. Whaley, *J. Chem. Phys.*, 2004, **121**, 4180.

54 J. K. G. Watson, *J. Chem. Phys.*, 1967, **46**, 1935.